DEBRIS BED HEAT REMOVAL MODELS: BOILING AND DRYOUT WITH TOP AND BOTTOM COOLING*

R. J. Lipinski and J. B. Rivard

Sandia Laboratories, Albuquerque, New Mexico 87185

ABSTRACT

A one-dimensional deep bed model for incipient dryout is developed which predicts deep bed behavior but not shallow bed behavior. A fluidization criterion results which indicates that a debris bed cannot be fluidized by the vapor flow. However, the maintenance of channels within the bed is predicted. A top-subcooled bed model is presented and evidence (both experimental and calculational) is given that the top-subcooled zone removes heat in series (not in parallel) with the boiling zone for sodium-cooled systems. The Sandia D-2 and D-3 top-subcooled dryout data is expressed in terms of non-subcooled dryout and compared with experimental data and model predictions from the literature. The data agrees with several predictions depending on whether the dryout in the boiling zone is dependent on the overlying subcooled zone thickness. A bottom-subcooled bed model is also presented. A post-dryout model is developed to explain the stable dry zone observed in the D-3 experiment and agreement with the data is found. Finally, the top-subcooled and post-dryout models developed are used to make predictions for the upcoming D-4 experiment.

INTRODUCTION

In the event of a severe accident in a fast reactor, molten core materials may contact liquid sodium, resulting in rapid quenching, freezing, and fragmentation of the core debris. Particulated fuel and steel may subsequently settle on available surfaces (including core catchers) within the reactor vessel, forming debris beds. The fuel in these debris beds will be heated by radioactive decay of retained fission products and actinides. The hazard level which should be assigned to the resulting post-accident condition depends on the extent to which natural cooling of the debris may be relied upon. This cooling depends partly on whether the liquid above the bed is at the saturation temperature or subcooled below that temperature, and whether the bed is resting on an insulating base or on a base with significant downward heat removal. This paper considers incipient bed dryout for all these cases (non-subcooled, top-subcooled, and bottom-subcooled beds) and also considers conditions beyond incipient dryout.

NON-SUBCOOLED BEDS

Most work on debris bed dryout has been concerned with bottom-insulated beds where the overlying liquid is at the saturation temperature (non-subcooled beds). In these beds, heat removal is entirely by latent heat transport. Extensive

---

*This work supported by the U. S. Nuclear Regulatory Commission.

experimental work has been performed with various materials, for both bottom and volumetric heating, and with the heat source both in the liquid and in the particles.[1-4] It has been observed that for deep beds, the heat flux at dryout is independent of bed depth, but for shallow beds, the dryout heat flux increases with decreasing bed depth. Vapor channels free of particles have been observed in the top portion of the beds, and it has been suggested that the resulting enhancement of vapor removal is the basis for the shallow bed behavior.[1-3]

Various models have been developed to explain deep and shallow bed behavior[2,3,5] however none of the deep-bed models included depth dependence explicitly in their derivation. Thus it remained to be seen whether a one-dimensional deep bed model could describe shallow bed behavior as depth decreased. The deep-bed model derivation of Hardee and Nilson[7] was expanded to one dimension. Defining z as the height above the bottom of the bed and as the fraction of the space between particles which is liquid (with the other variables as listed in the Nomenclature), the depth-dependent conservation equations are:

$$S = \rho_l h \frac{d}{dz} (\gamma V_l) \tag{1}$$

$$V_l = \frac{\kappa}{\mu_l}\left(-\rho_l g - \frac{dP}{dz}\right) \tag{2}$$

$$V_v = \frac{\kappa}{\mu_v}\left(- \frac{dP}{dz}\right) \tag{3}$$

$$\frac{d}{dz}\left((1 - \gamma)\rho_v V_v + \gamma \rho_l V_l\right) = 0 \tag{4}$$

The equations reduce to

$$S = \rho_l h \frac{d}{dz}\left(\frac{\gamma g \kappa}{\nu_l + \gamma \nu_v / (1 - \gamma)}\right) \tag{5}$$

With a uniform source S, equation (5) may be integrated and an explicit form for the liquid fraction γ is obtained:

$$\gamma = \beta \pm \sqrt{\beta^2 - S\nu_l z/(\rho_l^2 g\kappa h)} \tag{6}$$

where

$$\beta = 1/2 - (\nu_v/\nu_l - 1)S\nu_l z/(2\rho_l g\kappa h) \tag{7}$$

This function is plotted in Figure 1 for a bed at the dryout power and at one-half the dryout power. Each power has two solutions, one where the heat removal is limited by liquid downflow and one limited by vapor upflow. Only the vapor-flow limiting condition (where $\gamma = 1$ at the bed bottom) is thermally stable against perturbations in γ. As the power is increased, the liquid fraction in the stable solution decreases to allow more space for vapor removal. Dryout occurs when the increasing vapor fraction begins to choke off the downward liquid flow. The heat flux which exits from the top of the bed may be determined by integrating equation (5) from the bottom to the top of the bed, and the dryout heat flux is then obtained (similar to reference 5) by maximizing the heat flux with respect to variation in the liquid fraction. The result is:

$$q_d = (\rho_l g\kappa_t h/\nu_v)/(1 + \sqrt{\nu_l/\nu_v})^2 \tag{8}$$

which is essentially the same dryout heat flux obtained by Hardee and Nilson for saturated beds and does not show length dependence. Note that the permeability is evaluated at the top of the bed. Since the permeability is proportional to the square of the particle diameter, equation (8) implies that the dryout flux for a deep stratified bed, in which the smaller particles are at the top,[7] will be less than for an unstratified bed. This effect may be mitigated by channels penetrating the small-particle zone, but the effect should prevail in the limit of very deep beds. Exactly the same dryout flux is obtained if Joule-heating of the liquid only is modeled, as has been verified experimentally for deep beds.[4]

The fact that equation (8) does not predict a depth-dependent dryout flux suggests that another mechanism is required to explain shallow bed behavior. As mentioned earlier, Dhir and Catton[2,3] developed a model involving vapor channels free of particles within the bed. They stated that fluidization would occur in the upper portion of the bed, and indeed the model depended on the achievement of an optimal potential energy in the fluidization process in order to obtain the proper depth dependence observed in shallow beds. However, the model depicted the region between particle-free channels as being fluidized with liquid flowing downward, which is obviously impossible. Furthermore, one may use the one-dimensional model to calculate the potential for a deep bed to fluidize. The vapor velocity in the bed may be determined to be:

$$V_v = \frac{\rho_l g K}{\nu_v \rho_v}\left(1 - \frac{1}{1 + (\nu_v/\nu_l)(\gamma/(1 - \gamma))}\right) \qquad (9)$$

The vapor velocity at dryout may be combined with the bed fluidization criterion of Wallis[6] to yield the fluidization condition:

$$\rho_l > \rho_p(1 - \varepsilon)(1 + \sqrt{\nu_l/\nu_v}) \doteq \rho_p(1 - \varepsilon) \qquad (10)$$

As can be seen, the bed permeability cancels and the equations are reduced to the requirement that the fluidized particles be supported by the pressure generated from the weight of the liquid in the bed. This condition requires unreasonably large inter-particle volume fractions ca. 93% for sodium-UO_2 systems and 90% for water-steel systems. Thus the beds for which fluidization is assumed, fail to meet the above fluidization criterion by a wide margin.

Even though debris beds may not fluidize, the formation of channels has been observed by several experimenters.[1,3] The mechanism for channel formation is as yet uncertain. However, once a channel is formed, the vapor velocity through it would be greater for a given pressure drop than through a packed bed. This higher velocity could then levitate and remove any particle which entered the channel, thus maintaining the channel. Using the Hagen-Poiseulle law for pressure drop in a pipe and the single particle terminal velocity formula from Wallis[6], the criterion for a channel of diameter d_c to allow levitation of a particle of diameter d_p is found to be

$$d_c > (4/3)\sqrt{\rho_p/\rho_l}\; d_p \qquad (11)$$

For a water-UO_2 bed, the critical channel diameter for channel maintenance is four particle diameters, or about 2.0 mm. Channels of 2.5 mm diameter in water-UO_2 beds have been noted in reference 1.

TOP-SUBCOOLED BEDS

If the liquid overlying a debris bed is below the saturation temperature (subcooled), then the heat removal will be enhanced and the dryout flux increased.

Rivard[8] observed that the high conductivity of sodium and the large resistance to flow presented by a debris bed makes conduction a dominant heat removal mechanism. He suggested that there would be a zone of subcooled debris above the boiling zone in which heat removal could be modeled by conduction in series with heat removal from the boiling zone. Augmentation by single-phase convection could be accommodated by use of an enhanced conductivity. The relation between the total dryout flux in a top subcooled bed and the dryout flux for a non-subcooled bed is then

$$q_{d,ts}^2 = q_{d,ns}^2 + 2k_e(T_b - T_t)S \qquad (12)$$

Le Rigoleur[9] also considered heat removal by conduction in series and in addition considered heat removal from the subcooled zone in parallel with that from the boiling zone.

The choice between heat removal in series or in parallel with the heat from the boiling zone suggests a model in which the rising vapor either condenses quickly in the subcooled zone or penetrates to the overlying liquid. The condensation rate at a given point in a channel may be determined from the condensation flux and liquid-metal condensation coefficient given in Collier[10] and the semi-empirical formula for sodium saturation pressure[11]:

$$j = \frac{39.2\sqrt{\sigma}}{2 - 19.6\sqrt{\sigma}} F \sqrt{\frac{M}{2\pi R}} \left[\frac{\alpha e^{-\theta/T_v}}{T_v} - \frac{\alpha e^{-\theta/T_l}}{T_l} \right] \qquad (13)$$

where the dimensions are SI, $\alpha = 2.39 \times 10^{11}$ Pa · $K^{1/2}$ and $\theta = 12819$ K. Assuming the maximum observed sodium-UO_2 saturated dryout flux[1] of 1 MW/m^2 and 2.5-mm diameter channels spaced every 400 mm^2 (as observed in water-UO_2 systems[1]), the entire vapor flux would condense in about 5 mm. One would thus expect conduction in series to be the appropriate model for most subcooled beds in sodium.

The only particle-heated subcooled sodium-UO_2 dryout experiments performed to date have been the in-pile fission-heated D-series experiments performed at Sandia.[8,12,13] One may use the temperature measurements in those experiments to compare the series and parallel conduction models. In all of the runs the conduction zone length predicted by the parallel model exceeds the length of the subcooled zone as determined by the temperature measurements. On the other hand, the series conduction model fits the measured temperatures at dryout fairly well if an enhanced bed conductivity (due to convective effects) is used.[8] Thus, the series conduction model best agrees with the experimental data. The enhanced conductivity for the experiments was estimated to be 31, 36, and 43 W/m·K for bed depths of 58, 106, and 158 mm, respectively. This leads to an empirical relation for the effective conductivity at dryout as a function of bed depth:

$$k_e = 24 + 120L_T \qquad (14)$$

This is somewhat higher than the values suggested by single-phase convection correlations.[5]

One may now derive relations for top-subcooled dryout based on series conduction and non-subcooled dryout data. However, there is ambiguity about the appropriate bed depth to use to determine $q_{d,ns}$ in equation (12): the length of the boiling zone alone, or the total bed depth. For example, if channels within the boiling zone dominate the heat removal, then the appropriate length would be the boiling zone length. Conversely, if the total bed weight dictates dryout behavior, then the appropriate length would be the total bed depth. Therefore, two models for top-subcooled were developed, called the dependent and independent models (for boiling-zone or total-depth dependence, respectively.) For very deep beds, both models give the same result since then the non-subcooled dryout flux is independent of length.

The non-subcooled dryout flux may be expressed as a linear relation over the region of interest:

$$q_{d,ns,v} = a_v - b_v L \tag{15}$$

(For deep beds, b_v will be zero). Then the bed depth yielding dryout with the independent subcooled model is

$$L = \sqrt{(a_v/(S + b_v))^2 + 2k_e(T_b - T_t)/S} \tag{16}$$

and the depth which yields dryout with the dependent model is

$$L = \frac{(a_v b_v) \pm \sqrt{(a_v b_v)^2 - (a_v^2 + 2k_e(T_b - T_t)S)(b_v^2 - S^2)}}{b_v^2 - S^2} \tag{17}$$

(The positive root is used for $S > b_v$ and the negative root for $S < b_v$.)

One may now use the series conduction model to compare non-subcooled dryout data and models with the Sandia subcooled dryout data.[6] For convenience, rather than inserting the non-subcooled dryout relations into equations (16) and (17), the subcooled data can be unfolded via equations (12) and (14) (and the McDonald-Connolly relation[1] for the boundary layer temperature drop in the sodium) to obtain non-subcooled dryout fluxes for direct comparison. The unfolded data is presented in Figure 2, with each dryout flux plotted at two possible dryout lengths (total bed depth and boiling depth). Shown for comparison are curves fitting the data of reference 1 (in which Joule heating of sodium with UO_2 particles was used), the shallow bed model predictions of reference 3, and the deep bed model predictions of references 3 and 5 (using a nominal permeability of 1.5×10^{-10} m^2). There are three dryout data points (D-2a, D-3a, and D-3b) and one dryout lower limit (the "post-disturbance" D-2b). Three of the points agree with the reference 1 data if the dependent model is used, three agree with the reference 3 shallow bed model if the independent model is used, and three agree with the deep bed models of references 3 and 5 (using either subcooled model) if the bed permeability is 1.0×10^{-10} and 7.2×10^{-10} m^2, respectively. (These permeabilities correspond to effective particle diameters of 271 and 630 μm, respectively). Thus the data *does not clearly indicate at this point which subcooled model should be used.*

BOTTOM-SUBCOOLED BEDS

If the debris bed is resting on a structure capable of removing heat downward, significant additional heat removal can be achieved. Rivard proposed[10] that a subcooled zone will exist at the bottom portion of such a bed. Because the upper portion of the zone will be at a higher temperature, the sodium will not convect and the zone may be modeled with conduction independent of the upper zones. If the supporting structure is several centimeters of steel, allowance must be made for the significant temperature drop which can occur across it. Reducing the conduction equations, the dryout depth for a bed resting on a plate of thickness L_{pl} may be determined to be

$$L_T = L_{bs} + L_u \tag{18}$$

where the bottom-subcooled zone thickness L_{bs} is

$$L_{bs} = -(k_m L_{p1}/k_{p1}) + \sqrt{(k_m L_{p1}/k_{p1})^2 + 2k_m(T_b - T_{pb})/S} \qquad (19)$$

and the upward heat flow zone thickness L_u is determined by equations (16) or (17) for the independent and dependent top-subcooled models, respectively.

Figure 3 displays the power vs. total bed depth at dryout for a sodium-UO$_2$ bed on a 20-mm thick steel plate subcooled above and below by 400K using the dependent (upper) and independent (lower) top-subcooled models (with the non-subcooled dryout curves of references (1) and (3), respectively). The dryout bed depths without bottom subcooling are also shown (using equations (16) and (17)). As can be seen, bottom cooling can increase the dryout bed depths or powers by up to a factor of two. This is a strong incentive for the investigation of bottom-cooled in-vessel core catchers.

POST DRYOUT

In the Sandia sodium-UO$_2$ D-3 experiment[8,13] a stable dry zone at the bottom of the bed (with a stable boiling zone above it) was maintained at a power level slightly above dryout. This effect can be understood in terms of shallow bed behavior, since a thinner boiling zone can transport more heat through itself. A model was developed with a conducting dry zone underlying a boiling zone. Since the heat generated in the dry zone is delivered by conduction to the bottom of the boiling zone, the boiling zone is part bottom-heated and part volume-heated. However, the dryout flux for non-subcooled bottom-heated beds is different than that for volume-heated beds (see Figure 4). Thus the dryout flux was determined by linearly combining the non-subcooled volume-heated and bottom-heated dryout relations in proportion to the boiling and dry zone thicknesses, respectively:

$$SL_T = \frac{L_b}{L_T}\, q_{d,ns,v}(L_b) + \frac{L_d}{L_T}\, q_{d,ns,b}(L_b) \qquad (20)$$

To simplify the algebra, the dryout fluxes were assumed to vary linearly with length over the region of interest, with $q_{d,ns,v}$ determined by equation (15) and

$$q_{d,ns,b} = a_b - b_b L \qquad (21)$$

The dry zone length (for non-subcooled beds) was then determined to be

$$L_d = L_T - \lambda_{ns} - \sqrt{\lambda_{ns}^2 + \beta_{ns}} \qquad (22)$$

where

$$\lambda_{ns} = (a_v - a_b - b_b L_T)/(2(b_v - b_b)) \qquad (23)$$

$$\beta_{ns} = (a_b L_T - SL_T^2)/(b_v - b_b)) \qquad (24)$$

For a top subcooled bed, one may fold in the dependent and independent top-subcooled models previously described. With the independent subcooled model, the dry zone length is

$$L_d = \sqrt{L_T^2 - 2k_c(T_b - T_t)/S} - \lambda_{ns} - \sqrt{\lambda_{ns}^2 + \beta_{ns}} \qquad (25)$$

where λ_{ns} and β_{ns} are defined in equations (25) and (26). With the dependent subcooled model, the dry zone length is

$$L_d = L_T - \lambda_{ts} - \sqrt{\lambda_{ts}^2 + \beta_{ts}} \tag{26}$$

where

$$\lambda_{ts} = (a_v - a_b - b_b L_T - b_v L_{ts})/(2(b_v - b_b)) \tag{27}$$

$$\beta_{ts} = (a_b L_T - a_v L_{ts} - S(L_T - L_{ts})^2)/(b_v - b_b) \tag{28}$$

$$L_{ts} = L_T - \sqrt{L_T^2 - 2k_e(T_s - T_t)/S} \tag{29}$$

These models may now be compared to the D-3 data[8]. To adequately accommodate the effect of the vessel bottom heat losses and the noncentral location of the bottom thermocouple, the D-3 conditions were modeled with a general two-dimensional heat transfer code until a dry zone length was found which produced the observed temperatures. The results were that a power of 2.22 MW/m^3 (390 W/kg) produced a dry zone of 7.5 mm, and 2.33 MW/m^3 (410 W/kg) produced 8.6 mm (assuming a conductivity of 0.5 W/m$\cdot$K[15]). These two points define a line, the intercept of which (i.e., incipient dryout) has already been discussed in the section on top subcooling. The slope of the line is 1.6×10^{-8} m^4/W and is fairly insensitive to the intercept. The slope determined by the post-dryout model using the dependent top-subcooled model with reference 1 data is $1.8 \times 10^{-8} \times$ m^4/W. The slope using the independent top-subcooled model with the reference 3 model is 5.0×10^{-8} m^4/W. Considering the uncertainty in the data, the agreement with both models is reasonable.

D-4 PREDICTIONS

We are now in a position to make dryout and post-dryout predictions for the upcoming Sandia in-pile debris bed experiment, D-4. The experiment will use UO$_2$ particulate with the same size distribution and anticipated permeability as D-2 and D-3. The loading will be 450 kg/m^2 (~80 mm depth) and there will be dryout runs at two different subcoolings, as shown in Table I. The tests will be run at reduced pressures so that the bulk sodium may be close to saturation without excessively heating the vessel. There is some uncertainty on the effect of pressure on dryout. One deep bed model[5] predicts a nearly linear pressure dependence, while another[3] predicts none. Deep-bed experimental data displays pressure dependence ranging from none to the square root of pressure. There is unfortunately no shallow-bed dryout data with pressure variation, but the reference 5 model predicts a square root dependence. A fourth root dependence on pressure was assumed. The non-subcooled dryout data from reference 1 was for an interparticle volume fraction of 0.55. The dryout for a fraction of 0.43 (as in the D-3 and D-4 experiments) would be lower. Therefore, the slope of the volume-heated curve was reduced until it properly predicted the D-3 post dryout data (using the dependent subcooled model). The new curve (shown as a dashed line in Figure 4) was then attenuated by the fourth root of pressure and used to predict the D-4 dryout conditions. The reference 3 model predicts D-4 will be in the deep bed range (with no pressure dependence). A particle diameter of 0.271 mm best fits the D-3 and D-2 data with this model. This value was used with the reference 3 deep bed model and the independent top-subcooled model to make alternative D-4 predictions. (Because the bed is in the deep-bed regime, there is no post-dryout prediction). The predictions are shown in Table I.

TABLE 1

D-4 Experimental Conditions and Predicted Dryout States

Cycle	Bulk Sodium Temperature (K)	Saturation Pressure (kPa)	Predicted Dryout Power (MW/m^3)		Predicted Dry Slopes[a] (10^{-9} m^4/W)
			Dependent Model	Indep. Model	Dependent Model
1	573	18.0	11.0	8.5	144.
2	873	32.6	10.9	6.0	39.

[a] Change in dry zone thickness with respect to change in the volumetric heat source.

SUMMARY

A one-dimensional deep-bed model for incipient dryout has been developed which predicts deep-bed behavior but not shallow bed behavior. A fluidization criterion results which indicates that a debris bed cannot be fluidized by its vapor flow. However, the maintenance of channels within the bed is predicted. A top-subcooled bed model has been presented and evidence (both experimental and calculational) has been given that the top-subcooled zone removes heat in series (not in parallel) with the boiling zone for sodium-cooled systems. The Sandia D-2 and D-3 top-subcooled dryout data was expressed in terms of non-subcooled dryout and compared with the experimental data of reference 1 and the model predictions of references 3 and 5. The data agrees with all three references, depending on the value of permeability used and on whether the dryout in the boiling zone is dependent on the overlying subcooled zone thickness. A bottom-subcooled bed model has also been presented. A post-dryout model has been developed to explain the stable dry zone observed in the D-3 experiment and agreement with experimental data is found. Finally, the top-subcooled and post-dryout models developed have been used to make predictions for the D-4 experiment.

NOMENCLATURE

a	intercept of dryout curve (W/m^2)
b	slope of dryout curve (W/m^3)
C	specific heat ($J/kg \cdot K$)
d	diameter (m)
g	gravitational acceleration (m/s^2)
h	latent heat of vaporization (J/kg)
j	condensation flux ($kg/m^2 \cdot s$)
k	thermal conductivity ($W/m \cdot K$)
L	length or thickness (m)
M	molecular mass (kg/mole)
P	pressure (Pa)
q	heat flux (W/m^2)

Subscripts

b	boiling; bottom heating
bs	bottom-subcooled zone
c	channel
d	dryout;dry zone
e	enhanced
l	liquid
m	mixture of stagnant fluid and debris bed
ns	non-subcooled
p	particle

R	gas constant (J/K · mole)	pl	plate
S	volumetric heat source (W/m^3)	pb	plate bottom
T	temperature (K)	t	top of the bed
V	superficial velocity (m/s)	ts	top-subcooled zone
z	distance above the bed bottom (m)	T	total bed depth
γ	liquid fraction between particles	u	upward heat flow
ε	volume fraction of interparticle spaces	v	vapor; volume heating
κ	permeability (m^2)		
μ	dynamic viscosity (kg/m · s)		
ν	kinematic viscosity (m^2/s)		
ρ	density (kg/m^3)		

REFERENCES

1. J. D. GABOR, L. S. SOWA, L. BAKER, JR., and J. C. CASSULO, "Studies and Experiments on Heat Removal from Debris in Sodium," in *Proc. of ANS Fast Reactor Safety Meeting*, Beverly Hills, CA, CONF-740401 (1974), p. 825.

2. V. K. DHIR, I. CATTON, and W. E. KASTENBERG, Study of *Dryout Heat Fluxes in Beds of Inductively Heated Particles*, NUREG-0262, NRC-7 (1977).

3. V. K. DHIR and I. CATTON, "Prediction of Dryout Heat Fluxes in Beds of Volumetrically Heated Particles," *Proc. of Intern. Mtg. on Fast Reactor Safety and Related Physics*, Chicago, IL, CONF-761001 (1976), p. 2026.

4. L. S. SOWA, J. D. GABOR, L. BAKER, JR., J. R. PAVLIK, J. C. CASSULO, W. HOLLOWAY, "Studies of the Formation and Cooling of Particulate Fuel Debris beds in Sodium," *Proc. of Intern. Mtg. on Fast Reactor Safety and Related Physics*, Chicago, IL, CONF-761001 (1976), p. 2036.

5. R. C. HARDEE and R. H. NILSON, "Natural Convection in Porous Media with Heat Generation," *Nucl. Sci. and Eng.*, *63*, 119 (1977).

6. J. B. RIVARD and R. L. COATS, "Post-Accident Heat Removal: An Overview of Some In-Vessel Safety Considerations," (this meeting, section III-C).

7. G. B. WALLIS, *One-Dimensional Two-Phase Flow*, McGraw-Hill, New York (1966).

8. J. B. RIVARD, *Post-Accident Heat Removal: Debris Bed Experiments D-2 and D-3*, SAND78-1238 (1978).

9. C. LeRIGOLEUR, "Particle-Bed Dryout in Sodium", presented at *Fourth Post-*

10. J. G. COLLIER, *Convective Boiling and Condensation*, McGraw-Hill, New York (1976), p. 309.

11. R. W. DITCHBURN and J. C. GILMOUR, *Rev. Mod. Phys.*, *13*, 310 (1941).

12. J. B. RIVARD, *Debris Bed Studies and Experiments at Sandia Laboratories*, SAND78-0299 (1978).

13. J. B. RIVARD, "In-Reactor Experiments on the Cooling of Fast Reactor Debris," *Nucl. Tech.* (submitted for publication).

14. J. S. McDONALD and T. J. CONNOLLY, "Investigation of Natural Convection Heat Transfer in Liquid Sodium," *Nucl. Sci and Eng.*, *8*, 369 (1960).

15. H. G. PLEIN, R. J. LIPINSKI, G. A. CARLSON, and R. W. VARELA, "Summary of the First Three In-Core PAHR Molten Fuel Pool Experiments," (This meeting, section II-C).

Figure 1. Liquid fraction between particles vs. elevation

Figure 2. Unfolded dryout heat flux data from reference 6

Figure 3. Dryout depths with and without bottom cooling

Figure 4. Non-subcooled dryout heat flux vs. depth. Dashed line is the modified curve used in the D-4 predictions.

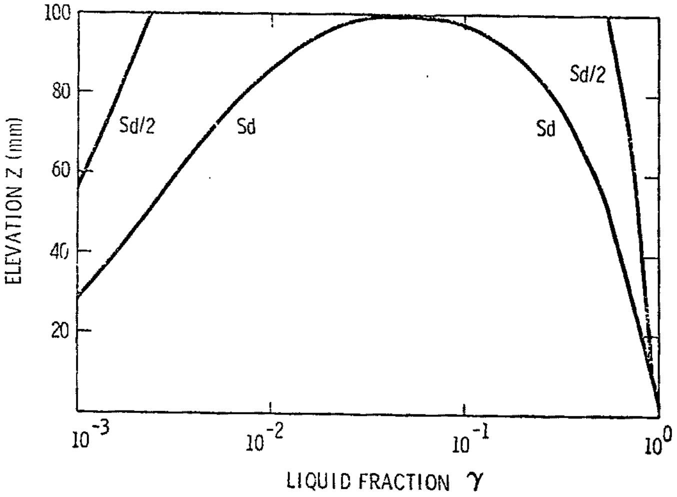
100
80
60
40
20
ELEVATION Z (mm)
Sd/2
Sd
Sd
Sd/2
10^{-3}
10^{-2}
10^{-1}
10^{0}
LIQUID FRACTION γ

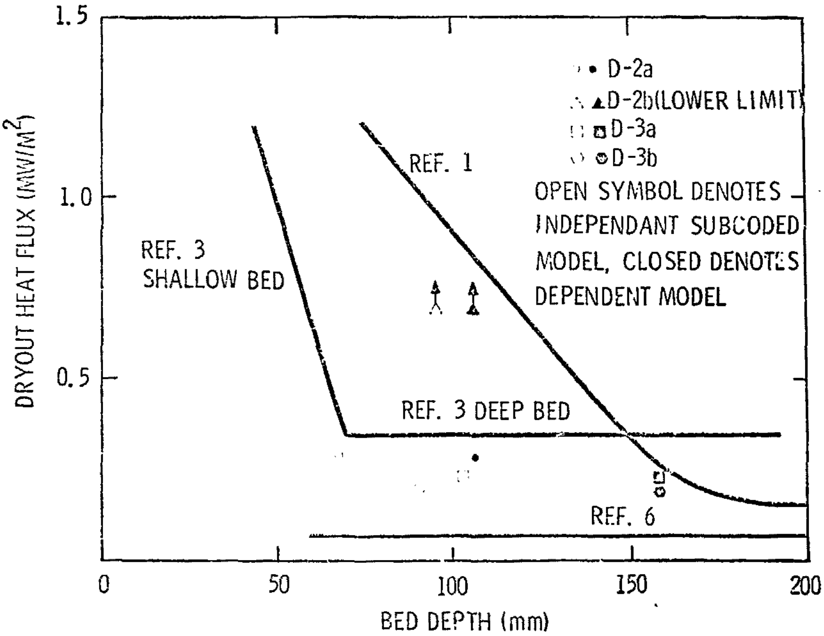
1.5
1.0
0.5
DRYOUT HEAT FLUX (MW/M²)
0
50
100
150
200
BED DEPTH (mm)
○ ● D-2a
△ ▲ D-2b(LOWER LIMIT)
□ ■ D-3a
○ ● D-3b
OPEN SYMBOL DENOTES INDEPENDANT SUBCODED MODEL, CLOSED DENOTES DEPENDENT MODEL
REF. 1
REF. 3 SHALLOW BED
REF. 3 DEEP BED
REF. 6

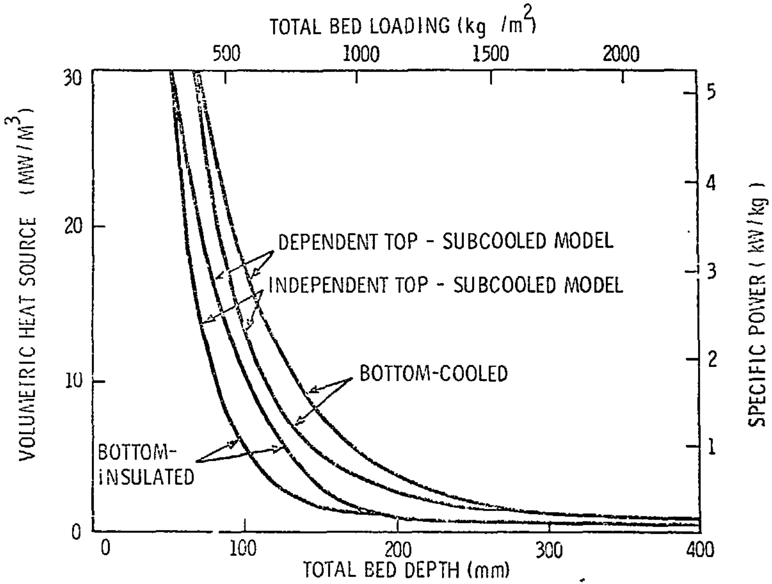
TOTAL BED LOADING (kg /m^2)
500
1000
1500
2000
30
20
10
0
VOLUMETRIC HEAT SOURCE (MW/M^3)
DEPENDENT TOP - SUBCOOLED MODEL
INDEPENDENT TOP - SUBCOOLED MODEL
BOTTOM-COOLED
BOTTOM-INSULATED
5
4
3
2
1
SPECIFIC POWER (kW/kg)
0
100
200
300
400
TOTAL BED DEPTH (mm)

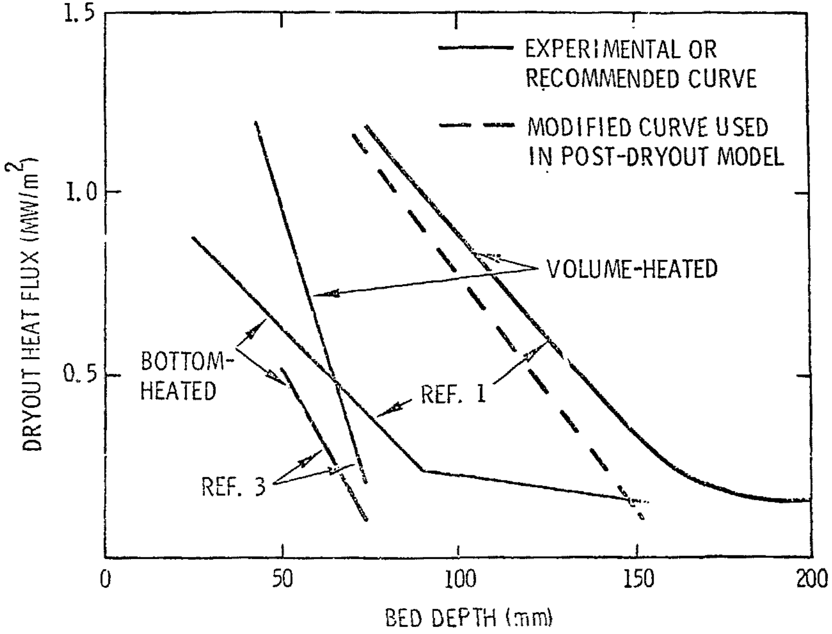

1.5
1.0
0.5
0
50
100
150
200
BED DEPTH (mm)
DRYOUT HEAT FLUX (MW/m^2)
EXPERIMENTAL OR RECOMMENDED CURVE
MODIFIED CURVE USED IN POST-DRYOUT MODEL
VOLUME-HEATED
BOTTOM-HEATED
REF. 1
REF. 3